ICES REPORT 13-33

December 2013

Computational and MR-guided Patient-Specific Laser Induced Thermal Therapy of Cancer

by

D. Fuentes, J. T. Oden, K. R. Diller, J. Yung, Y. Feng, J. D. Hazle, A. Shetty, and R. J. Stafford



The Institute for Computational Engineering and Sciences
The University of Texas at Austin
Austin, Texas 78712

Reference: D. Fuentes, J. T. Oden, K. R. Diller, J. Yung, Y. Feng, J. D. Hazle, A. Shetty, and R. J. Stafford, Computational and MR-guided Patient-Specific Laser Induced Thermal Therapy of Cancer, ICES REPORT 13-33, The Institute for Computational Engineering and Sciences, The University of Texas at Austin, December 2013.

Computational and MR-guided Patient-Specific Laser Induced Thermal Therapy of Cancer

D. Fuentes, J. T. Oden, K. R. Diller, J. Yung, Y. Feng, J. D. Hazle, A. Shetty, and R. J. Stafford

Abstract This chapter describes the development of a canonical dynamic data driven predictive control system for MR-guided laser induced thermal therapies (MRgLITT) of focal cancerous lesions within soft tissue. The predictive ability of computational models combined with advanced clinical imaging modalities is exploited to plan, predict, control, and optimize the treatment outcome. The system is under continual development and embodies a cyberinfrastructure comprised of Magnetic Resonance Thermal Imaging (MRTI), computer visualization, laser optics, nonlinear dynamic bioheat transfer models of heterogeneous tissue, adaptive meshing, high-performance parallel computing, cell-damage models, inverse analysis, model validation, signal processing, optimal control algorithms, and error estimation. These diverse technologies and systems are connected across high-speed networks and is an excellent example of a Dynamic Data Driven Application System (DDDAS).

Webpage: `http://wiki.ices.utexas.edu/dddas`

D. Fuentes, J. D. Hazle, A. Shetty, R. J. Stafford, and J. Yung
The University of Texas M.D. Anderson Cancer Center, Department of Imaging Physics, Houston TX 77030, USA, e-mail: `[dtfuentes,jhazle,anil.shetty,jstafford,jyung]@mdanderson.org`

Y. Feng,
Computational Bioengineering and Nanotechnology Lab, The University of Texas at San Antonio, San Antonio, TX 78749, USA, e-mail: `yusheng.feng@utsa.edu`

K. R. Diller
Department of Biomedical Engineering, The University of Texas at Austin, Austin TX 78712, USA, e-mail: `kdiller@mail.utexas.edu`

J. T. Oden
Institute for Computational Engineering and Sciences, The University of Texas at Austin, Austin TX 78712, USA, e-mail: `oden@ices.utexas.edu`

1 Introduction

Laser induced thermal therapy (LITT) is a minimally invasive procedure that replaces the scalpel of conventional surgery and the ionizing radiation of radiosurgery with a $<$2mm laser diode applicator minus the typical side effects and morbidity. A specially designed laser fiber is delivered stereotactically or under real-time image-guidance to the site of a tumor. The fundamental idea is that when the laser heats the tumor cells to a certain point, the cells are damaged and die. The heating portion of the procedure takes only a few minutes. MR-guided LITT (MRgLITT) is performed under thermal image monitoring using magnetic resonance thermal imaging (MRTI). The thermal images provide a quantitative treatment time estimate of the lethality of the thermal dose received by the tumor and surrounding healthy tissue. Multiple post market studies [5, 6, 4, 25, 8] are currently on-going for FDA cleared MRgLITT systems in humans (Visualase®, BioTex Inc.; Monteris Med., Neuroblate®). The MRgLITT systems utilize real-time temperature imaging feedback and dosimetry.

While real-time temperature monitoring provides invaluable treatment-time feedback that makes the procedure safe and feasible once a laser applicator has been placed, innovations in human assisted high performance computational tools using this feedback are under development to plan, control, predict, and optimize the anticipated biological response to dramatically increase treatment efficacy and reduce associated treatment morbidity and even reduce recurrence of the disease.

DDDAS aims at developing a computational system that dynamically interacts with medical imaging technology for the predictive guidance and control of medical procedures. It is a monumentally important development that could enhance many fields of medical science. The unique dynamic closed loop control system presented by the predictive capabilities of computational simulation coupled with real-time multi-planar image guidance as feedback has significant potential to facilitate a reliable minimally invasive treatment modality that delivers an optimized thermal dose prescribed by the physician. The control system developed in this work, Figure 1, employs a cyberinfrastructure [1] of magnetic resonance thermal imaging, computer visualization, laser optics, high-speed networks, nonlinear dynamic bioheat transfer models of heterogeneous tissue, adaptive meshing, high-performance parallel computing, cell-damage and heat-shock protein models, inverse analysis, calibration, model validation, signal processing, optimal control algorithms, and error estimation and control. The imaging system manages the thermal data and laser source and is connected over a high bandwith network to computational infrastructure that uses parallel computing algorithms to generate and solve computational models of bioheat transfer and visualization software to interactively visualize the procedure. The governing Pennes bioheat transfer constrained optimization equations are reviewed in Section 2. The workflow and treatment protocols of the computer driven

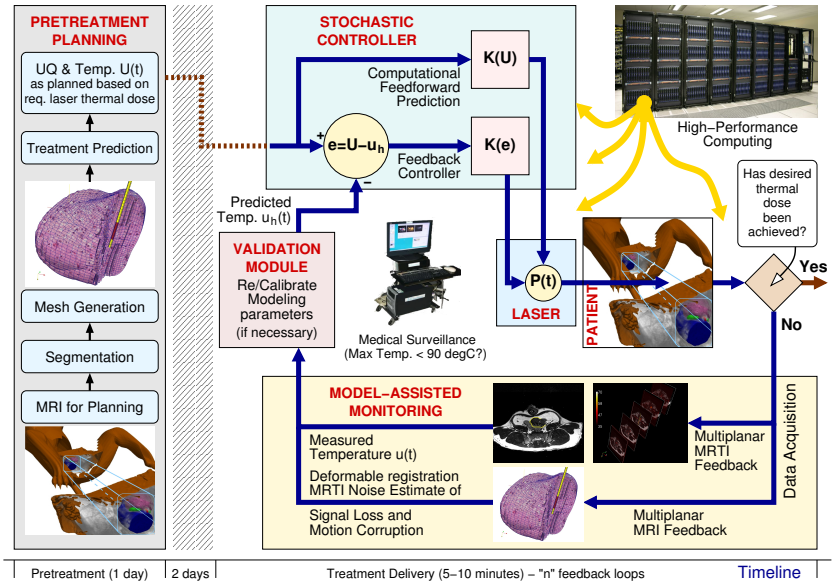


Fig. 1 The flowchart depicts the components that constitute computer assisted MRgLITT. 1) Treatment planning [21, 11] (on the left) is necessary for integration of imaging information and 3D modeling to provide the best guess at how to approach the therapy and assess potential problems in the safety and efficacy of the procedure ahead of time. 2) Model-assisted monitoring [22] (bottom) provides a quantitative data assimilation framework for integrating noisy real-time temperature imaging with computational prediction to provide the best estimate of the temperature field during the therapy. 3) Ultimately, a dynamic controller [20] (top) compares the feedback-based predicted temperature with the planned temperature and allows for modulation of the control parameters of the laser in order to conform to the treatment plan while maintaining safe conditions. 4) The validation module (middle) combines imaging feedback with computer modeling in order to validate, and change if necessary, the computer model and to best assess the extent and potential outcome of therapy by providing predictive capabilities.

MRgLITT DDDAS research are described in the Section 3. MRgLITT DDDAS research results are recapitulated in Section 4. This chapter concludes with the authors' vision of the future direction towards realizing this technology within a general clinical setting.

2 Governing Equations

The equations of bioheat transfer and light transport within laser-irradiated tissue are the fundamental equations used in this work. Elements of continuum mechanics, thermodynamics, anatomy, and physiology are coalesced within the field of bioheat transfer. Biological heat transfer may include conduction, convection, radiation, metabolism, and evaporation. However, the defining characteristic is the biological

heat transfer between blood and tissue; blood flow through the complex vasculature networks embedded in tissue may act as a significant heat sink in MRgLITT. The seminal development of the equations of bioheat transfer are attributed to the work of Pennes [29] in 1948. The original Pennes model describes bioheat transfer as the conservation of energy applied to a motionless non-deforming homogeneous mass of human tissue. The model does not allow mass flux across the boundary and assumes a uniform heat source based on the perfusion of blood throughout the tissue. Pennes model has been shown to provide very accurate predictions of biological heat transfer [12, 17, 7, 13, 15, 27, 31, 37]. We employ a nonlinear modification of the Pennes model and allow the thermal conductivity and perfusion model parameters to vary spatially. The initial boundary value model is defined by the following system:

$$\begin{aligned}
&\rho c_p \frac{\partial u}{\partial t} - \nabla \cdot (k(\mathbf{x})\nabla u) + \omega(\mathbf{x}) c_{blood}(u - u_a) = Q_{laser}(\mathbf{x},t) \quad \text{in } \Omega \\
&Q_{laser}(\mathbf{x},t) = P(t)\mu_{eff}^2 \frac{\exp(-\mu_{eff}\|\mathbf{x}-\mathbf{x}_0\|)}{4\pi\|\mathbf{x}-\mathbf{x}_0\|} \qquad \begin{array}{l} \mu_{tr} = \mu_a + \mu_s(1-g) \\ \mu_{eff} = \sqrt{3\mu_a\mu_{tr}} \end{array} \\
&\qquad -k(\mathbf{x})\nabla u \cdot \mathbf{n} = h(u - u_\infty) \qquad \text{on } \partial\Omega_C \\
&\qquad -k(\mathbf{x})\nabla u \cdot \mathbf{n} = \mathscr{G} \qquad \text{on } \partial\Omega_N \\
&\qquad u(\mathbf{x},0) = u^0 \qquad \text{in } \Omega
\end{aligned} \tag{1}$$

The measured baseline body temperature is taken as the initial temperature field, u^0. The density of the continuum, ρ, is homogeneous and the c_{blood} denotes the specific heat. On the Cauchy boundary, $\partial\Omega_C$, u_∞ is the ambient temperature and h is the coefficient of cooling. $\mathscr{G}$ denotes the prescribed heat flux on the Neumann boundary, $\partial\Omega_N$. The classical spherically symmetric isotropic solution to the transport equation of light within a laser-irradiated tissue [36] is used to model optical-thermal response to the laser source, $Q_{laser}(\mathbf{x},t)$. The anisotropic factor is denoted g and $\mathbf{x}_0$ denotes the position of laser photon source. $P(t)$ is the laser power as a function of time, μ_a and μ_s are laser coefficients related to laser wavelength and give probability of absorption and scattering of photons, respectively. The perfusion, $\omega(\mathbf{x})$, and thermal conductivity, $k(\mathbf{x})$, are allowed to vary spatially within a local region of interest, $r \approx 1cm$, around the laser source.

$$k_0(\mathbf{x}) = \begin{cases} k_0, & x \notin \mathscr{B}_r(\mathbf{x}) \\ k_0(\mathbf{x}), & x \in \mathscr{B}_r(\mathbf{x}) \end{cases} \qquad \omega_0(\mathbf{x}) \begin{cases} \omega_0, & x \notin \mathscr{B}_r(\mathbf{x}) \\ \omega_0(\mathbf{x}), & x \in \mathscr{B}_r(\mathbf{x}) \end{cases}$$

The main problems of the control system are the optimal control of the laser source and the calibration of the model parameters with respect to thermal imaging data. The mathematical structure of the calibration and optimal control problems both fall within the framework of PDE constrained optimization: Find the set of model parameters β^*, that minimizes a given objective function, Q, over a parameter manifold, $\mathbb{P}$,

$$\boxed{\begin{array}{l}\text{Find } \beta^* \in \mathbb{P} \text{ s.t.} \\ \qquad Q(u(\beta^*),\beta^*) = \inf_{\beta\in\mathbb{P}} Q(u(\beta),\beta)\end{array}}$$

Where β may represent any subset of the model parameters available for optimization, perfusion, thermal conductivity, and laser parameters are highlighted in (1), and the objective function, Q, is of the form of the $L_2(0,T;L_2(\Omega))$ norm of the difference between the predicted temperature field, $u(\mathbf{x},t)$ and an ideal temperature field $u^{\text{ideal}}(\mathbf{x},t)$.

$$\begin{aligned} Q(u(\mathbf{x},t)) &= \frac{1}{2}\|u(\mathbf{x},t) - u^{\text{ideal}}(\mathbf{x},t)\|^2_{L^2(\Delta T;L^2(\Omega))} \\ &= \frac{1}{2}\int_\Omega \int_{\Delta T} \left(u(\mathbf{x},t) - u^{\text{ideal}}(\mathbf{x},t)\right)^2 \, dtdx \end{aligned} \tag{2}$$

where $dx = dx_1 dx_2 dx_3$ is a volume element and the time interval of interest is denoted ΔT. u^{ideal} may represent the thermal imaging data for the calibration problem or a desired thermal dose for the optimal control problem. A quasi-Newton optimization solver [3, 18] is used for the PDE constrained optimization problems. The gradient of the objective function (2) is computed using an adjoint method. The derivation of the gradient may be found in [16, 28].

3 Simulation Guided MRgLITT Workflow

An overview of the treatment workflow is provided in Table 1. T_1 and T_2-weighted magnetic resonance (MR) imaging allows targeting of the treatment site and surrounding critical structures. In addition, MR imaging provides the ability for real-

Table 1 Treatment Workflow

Pretreatment	Image Acquisition Optimizations Model Predictions	Geometry Extraction Surgeon Interaction
Treatment Setup	Registration Model Predictions	Patient Specific Calibrations Treatment Day Updates
Inter-operative	Real-Time Monitoring Model Updates	 Model Control of Delivery
Post Treatment	Prediction Validation	

time feedback and post-treatment imaging verification of thermal therapy delivery. Several days prior to treatment, the anatomy, the prostate in this case, is scanned using a clinical MR scanner. This pre-operative, anatomical data is used to create a 3D finite element representation of the geometry of the anatomy, Figure 2. A pipeline of software is used to segment the anatomy, create a faceted surface representation, and generate a high-quality finite element mesh. An experienced user must identify and

extract the geometry from the pre-operative images. The facetted surface represents a 3D manifold that is then used to create a volumetric finite element mesh.

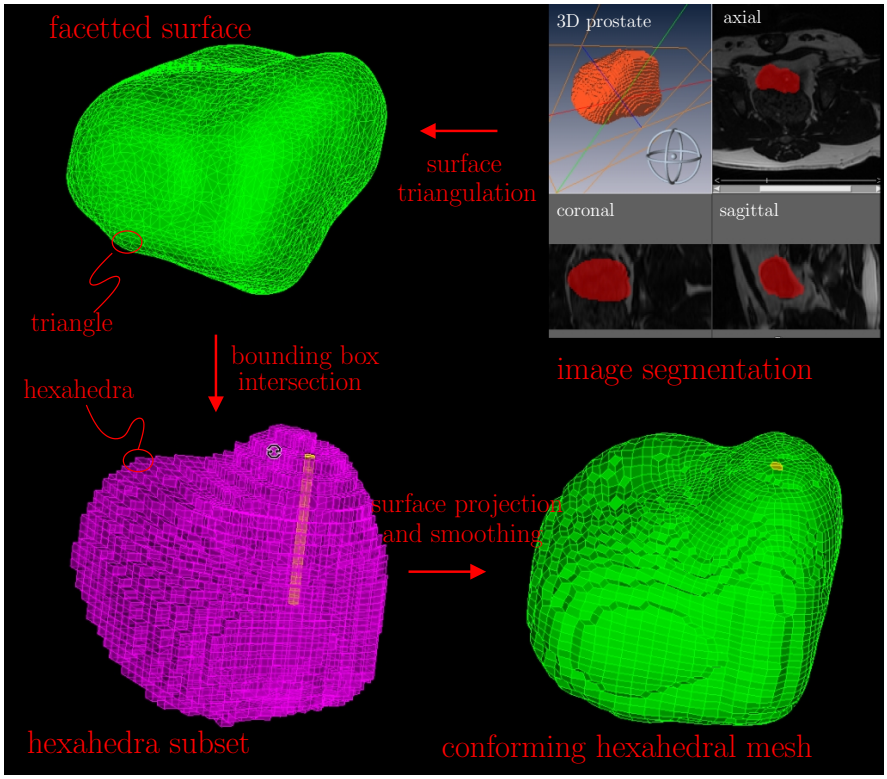


Fig. 2 Anatomical imaging to hexahedral finite element mesh pipeline. The anatomy of interest is labeled for segmentation. The prostate is labeled using a subset of the axial images. The anatomy labels are displayed in the coronal and sagittal planes as well to ensure 3D conformity to the boundary of the anatomy. The labeled voxels corresponding to the prostate are displayed in 3D and a facetted triangulation representing the boundary of the prostate is generated. The intersection of a structured grid and the volume enclosed by the interior of the facetted surface is the base of the hexahedral mesh. The surface of the initial hexahedral mesh is projected toward the boundary of the prostate and the mesh is smoothed.

Given the finite element mesh of the anatomy, initial optimal laser parameters are identified such as the location of the endpoint of the optical fiber and laser power as a function of time. Prior to treatment, mock simulations of the therapy are performed using tabulated bioheat transfer data, Figure 3, and allow the physician to tune the computed optimal delivery. The laser is placed in the prostate using a stereotactic guide. An actively cooled applicator with 980nm diffusing tip fiber is used to deliver therapy. Laser power is controlled by sending updated powers to the commercial MRgLITT delivery system in real-time. The initial parameters are corrected during the calibration phase of the process using MRTI generated thermal imaging

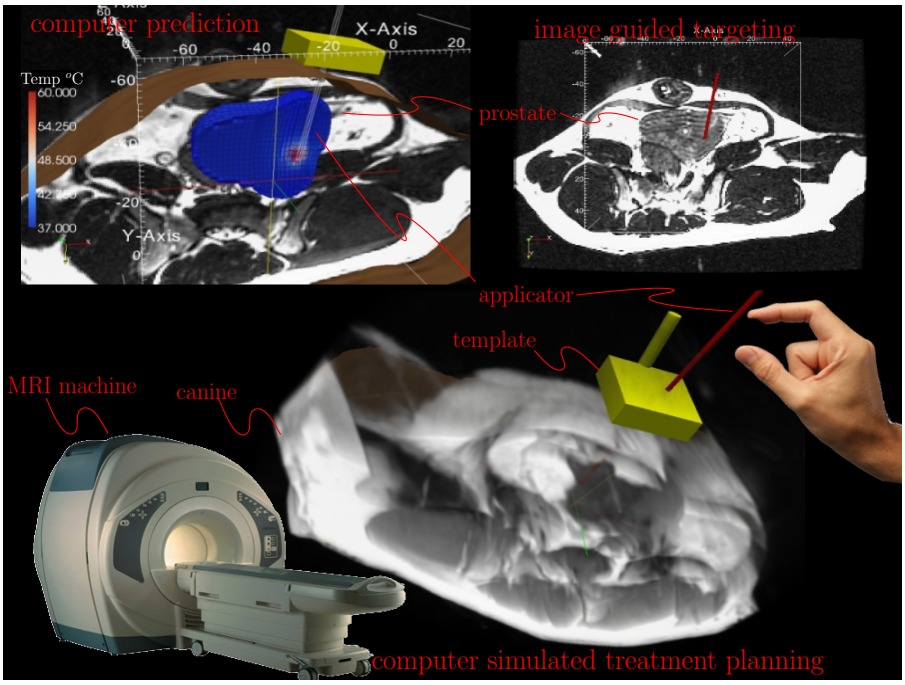


Fig. 3 Computer guided treatment planning. A fiducial marked treatment template is registered to planning images and used to guide the laser applicator. Prior to the procedure, trial simulations of the thermal delivery may be simulated to evaluate the effect of the desired thermal dose to surrounding critical structures. Virtual repositioning of the laser reduces the morbidity associated with physically repositioning the applicator.

data. Developed over the past decade, MRTI technology is a modification of existing MRI technology to use temperature sensitive echo planar imaging sequences to acquire larger imaging volumes in the same time with comparable temperature sensitivity and to provide a time varying multi-planar temperature field in the living tissue. The treatment control system is guided by computer simulation output. The simulation tools embed thermal imaging data within a Pennes bioheat transfer model constrained optimization framework. Through accurate computer prediction, the bioheat transfer response may be controlled through a collection of imaging based measurements about how the complex physiological system is responding to the surgery and make treatment plan updates based on an intelligent understanding of the physiological pathways to affect the surgical outcome.

4 Results

The DDDAS infrastructure for MRgLITT has been successfully tested *in vivo* canine prostate. The laser induced thermal therapy was performed at M.D. Anderson Cancer Center (MDACC) in Houston, Texas. A non-destructive calibration laser pulse was used to acquire intra-operative real time thermal imaging data of the heating and cooling and calibrate the computational models of bioheat transfer. The bioheat transfer was controlled to within 5°C of the predetermined treatment plan using the calibrated models implemented on high performance computing architectures. Real-time visualization of the anatomical data, thermal imaging data, FEM prediction, and model parameters of the on-going treatment was provided. The computational requirements imposed an 18 minute treatment time; 3 minutes for delivery of a low power training pulse, 5 minutes of actual therapeutic exposure, and the rest for synchronization and computational overhead. Post operative histology of the canine prostate reveals that the damage region was within the targeted 1.2cm diameter treatment objective. See [16, 20] for further technical details.

In vivo experiments thus far have utilized homogeneous parameter calibration techniques. Heterogeneous model calibration involving thousands of model parameters have been shown to deliver model predictions of unprecedented accuracy [9]. Recent work has demonstrated the feasibility of converging to a solution of a heterogeneous Pennes PDE constrained optimization problem with thousands of model parameters on the scale of minutes [19, 18]. Figure 4 shows the effect of calibrating the tissue models as a heterogeneous linearly conductive media. Allowing the biological thermal properties to vary spatially provides a means to achieve patient specific accuracy in the model prediction.

Current work is critically examining the accuracy of the predicted temperature distributions in the presence of uncertain input tissue parameters [11, 22]. This stochastic approach to bioheat simulation, includes parameter uncertainty and provides a probabilistic measure of the achievable damage. Unlike the classic deterministic approach, stochastic simulation provide a visualization of a volume that has a 95% probability of reaching tissue death, Figure 5. For data assimilation [22], the confidence levels add robustness to the temperature estimations in the presence of thermal imaging arftifacts. The primary goal, within the context of treatment planning, is to communicate the maximal potential extent of treatment for a specific patient and approach. There is little need to worry about the simulation leading to overtreatment as the real-time temperature imaging [33, 32] integrated into these procedures provides the physician with feedback for making the decision to cease treatment.

5 Discussion and Future Direction

Results have demonstrated the *feasibility* of designing simulation protocols and methodologies that interact with thermal imaging modalities and provide real-time

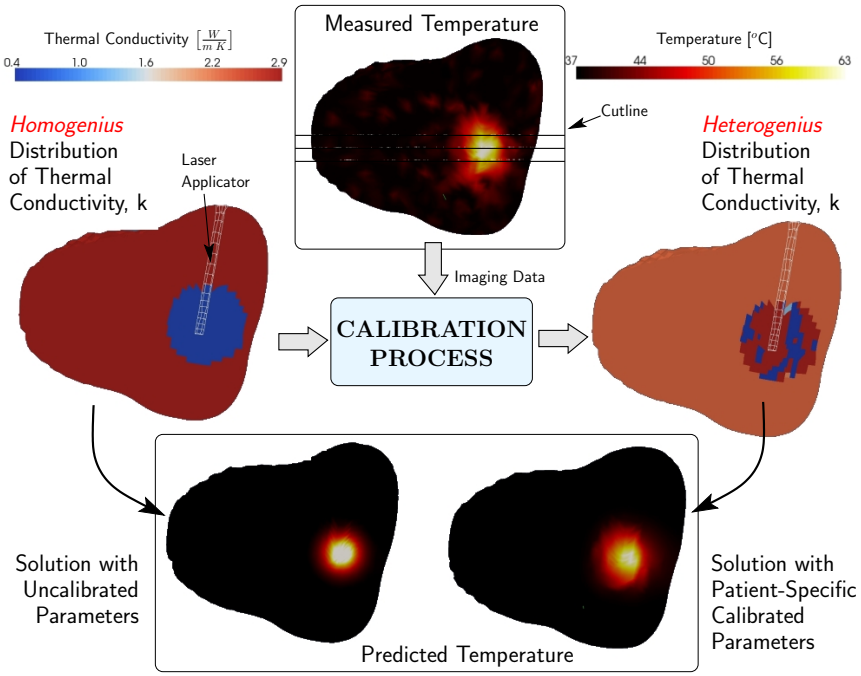


Fig. 4 Model calibration using homogeneous and heterogeneous model parameters [19]. A particular time instance of the thermal imaging data used to drive the model calibrations is shown at the top. The uncalibrated model begins with homogeneous model parameters with different coefficients in the neighborhood of the laser tip, left center. Isotherms of the initial uncalibrated temperature prediction are spherical, as expected from a homogeneous media with a isotropic source term, lower left. As the optimization process recovers spatially varying thermal parameters, center right, isotherms of the model prediction are no longer spherical and are in significantly much better agreement with the thermal imaging data.

control of thermal therapies for cancer treatment in a clinical setting. Calibration pulses prior to delivery of the thermal insult can be used to recover heterogeneous biothermal parameters on a patient specific basis. The predictive ability of computational models can be exploited to predict, control, and optimize the treatment. All necessary technologies to realize computer driven MRgLITT within a clinical setting setting currently exist; magnetic resonance thermal imaging, computer visualization, laser optics, high-speed networks, nonlinear dynamic bioheat transfer models of heterogeneous tissue, adaptive meshing, high-performance parallel computing, cell-damage and heat-shock protein models, inverse analysis, calibration, model validation, signal processing, optimal control algorithms, and error estimation and control. Substantial effort is needed to commercialize these technologies into streamlined computational tools similar to those that exist for stereotactic radiosurgery [35].

A hierarchical suite of computational tools for MRgLITT is needed, Figure 6. Computational tools for prospective 3D treatment planning of MRgLITT forms the

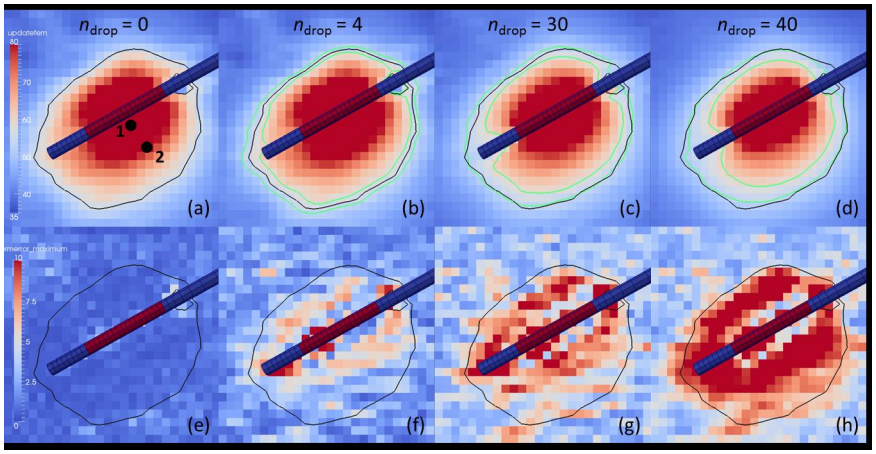


Fig. 5 Uncertainty quantification within a Kalman Filter frame work is shown under a systematic increase in data loss. Computationally efficient data assimilation techniques are under development and a current implementation that diagonalizes the covariance matrix is presented. Kalman temperature predictions are shown under an increasing simulated data loss. In total duration, 60 temperature measurements were acquired; (b) 7%, (c) 50%, (d) 66% data loss were simulated uniformly over time and compared to no data loss shown in (a). For comparison, the identical 57^{o}C MR temperature isotherm is shown in black and the green isotherms designate the 95% confidence interval of the predicted 57^{o}C isotherm in (a)-(d). Maximum pixel-wise error between the Kalman predictions and the MR temperature distributions for each corresponding simulated data loss is shown in (e)-(h). The maximum error for the Kalman prediction without any simulated data loss in (e) shows the uncertainty of the Kalman prediction process as a reference.

software foundation. Tools for prospective treatment planning are a necessary precursor to existing online temperature monitoring technologies. A significant software development effort is needed to streamline protocols and computational visualization interfaces to interact with existing stereotactic technology for treatment time positioning of the thermal applicator. For example, for thermal therapy of prostate, fiducials on the applicator can be registered to planning images and three dimensional visualizations of the anatomy, using either segmented surfaces or volume visualization techniques. The visualizations can provide depth perception for applicator insertion superior to current methodologies that use a series of 2D slices and have led to applicator insertion that can damage surrounding tissues. Further, given the projected applicator position, the thermal dose to the targeted lesion and other critical structures, seminal vesicles, rectum, bladder, may be simulated. Visualization of the percentage of target tissue predicted to have a lethal thermal damage by an Arrhenius model or a two-state model [14] with respect to the desired plan and visualization of surrounding structures, Figure 7, may reveal the necessity of repositioning the laser or early laser power cutoff. The software interface is a crucial component of the system. A user-friendly and portable software infrastructure that will cleanly interact with a variety of commercial imaging modalities will provide

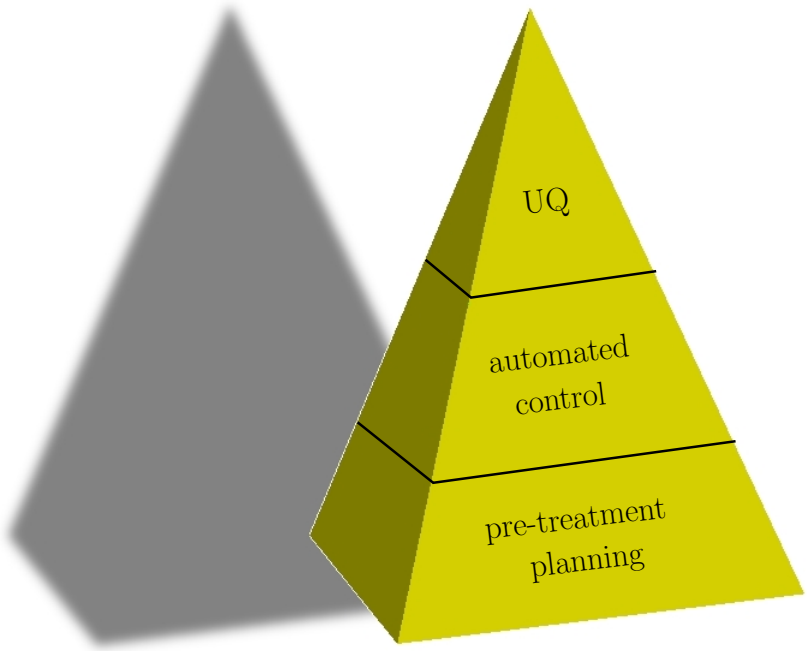


Fig. 6 The translational research involved to realize computer driven MRgLITT within a clinical setting will build upon a hierarchy of methodologies and technologies each increasing in complexity. The customized graphical user interface for visualizing and monitoring thermal image feedback along with computational predictions for pre-treatment planning provides the software foundation. The natural next layer of technology is provided by robust software for automated control of the thermal therapy delivery modality and updating the computational models on a patient specific basis. Software for uncertainty quantification (UQ)-based decisions and control provides the final step; the degree of confidence in the treatment success, including percentage of target lesion destroyed and an estimated damage to nearby critical structures, will allow surgical oncologists to make informed decisions.

a reproducible means of therapy and allow the construction of multi-institutional trials to evaluate this therapy versus conventional modalities.

A substantial amount of work is needed to retrospectively validate and verify the software predictions in phantoms and *in vivo*; the validated models can then be used to answer important therapeutic questions and evaluate the efficacy of the tool for deciding the placement and number of fibers needed to safely and effectively treat a target volume and decrease the need for retreatment and repositioning. Models that recover the patient specific thermal parameters have demonstrated significant potential in accurately predicting the bioheat transfer and have even been shown to compensate for modeling inaccuracies in the thermal source term. Experiments can be conducted that validate the spatially varying thermal parameters recovered by inverse problems against the actual local physical values. These experiments may

require accurate modeling of the laser fluence distribution beyond that provided by the isotropic source term presented in this work; either a Monte Carlo source [30] or delta-P[10] model may be needed. Physiological factors that locally change the perfusion levels can have a dramatic effect on the upper lesion size limits. Given an expected perfusion rate and the expected upper limit on lesion size, the necessity of using multiple laser applicators may be evaluated. Further, the efficacy in terms of conformal thermal dose and cost of multiple laser applicators can be compared to that obtained using a high laser power from a single applicator. Because of the uses of laser for therapy delivery, the use of nanoshells may play an important role in the future; an effective distribution of nanoshells that enhances the thermal properties of the media combined with a high laser power may prove to deliver an equivalent lethal conformal thermal dose as multiple applicators.

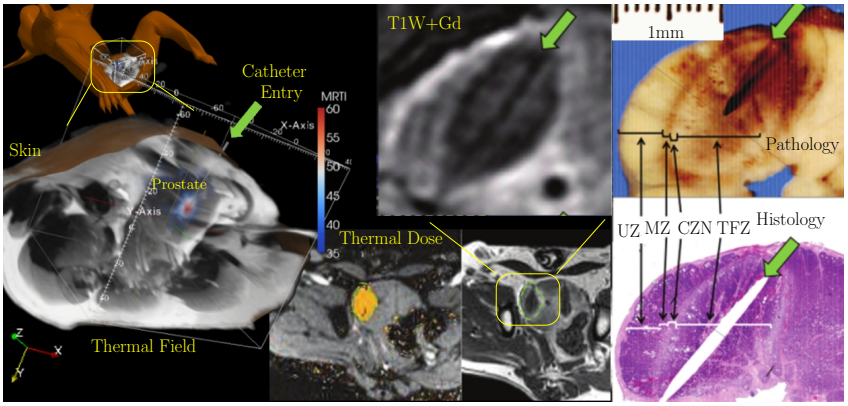


Fig. 7 Post Treatment validation. Post treatment contrast that enhances the T_1 properties of the tissue may be used to validate the damage predicted by an Arrhenius damage model. The arrows indicate the track of the applicator. The use of the T_1 enhanced region has been validated as a surrogate for tissue histo-pathology and correlations with the estimated damage corresponding to the Coagulative Necrosis Zone (CZN), Thermally Fixed Zone (TFZ), Marginal zone (MZ), and the Untreated zone (UZ) have been critically analyzed [33]. Using 3D visualization techniques, the damage region may be shown in perspective to the target tissue and surrounding structures.

As the planning software matures and is clinically validated, the computational performance and methodologies will be optimized for computer guided real-time delivery and control. The target of real-time control is to deliver a lethal thermal dose that conforms to the target lesion. Imaging feedback must be used with laser applicator(s) to update the bioheat transfer models to the biological thermal properties of the patient. The models will modulate the power delivered by applicator(s) to deliver a conformal lethal dose. Problems inherent to computer driven MRgLITT have been posed as PDE constrained optimization problems; within the perspective of a clinical setting, the overhead associated with the solution to these inverse problems requires at least an order of magnitude speedup to allow treatment protocol design that is able to calibrate and recompute optimal parameters instantaneously.

Alternative frameworks are being explored, such as state space control theory, to achieve the required performance. The likely solution will be a coalescence of multiple frameworks. Ultimately, efficient computational approaches for stochastic control are needed that embody useful statistical information within expected values and standard deviations of predicted treatment outcomes that are clinically familiar to physicians. Under the stochastic framework, the MRgLITT computational tools will provide a degree of confidence in the computational predictions directly proportional to the quality of the patient specific model parameters known at LITT time.

DDDAS methodologies combined with minimally invasive approaches to surgery have significant potential to dramatically improve cancer therapies and enhance the quality of life of cancer patients. A few of the many factors and complexities that must be overcome to advance this particular DDDAS implementation within a clinical setting has been presented. Current work focuses on LITT and MRTI as the thermal and imaging modalities, but the technology developed is adaptable to other MR-guided thermal therapies, such as focused ultrasound. Computationally, changing the thermal source or imaging modality amounts to utilizing a different source term in the governing PDE or adjoint problem, respectively. We are optimistic that these methodologies of computer modeling and simulation interacting with medical technologies have the potential to be extended to many target tissues and significantly enhance many areas of thermal therapy, including RF, microwave, ultrasound, and even cryotherapy applicators.

Acknowledgements The research in this chapter was supported in part through 5T32CA119930-03, 1R21EB010196-01, and K25CA116291 NIH funding mechanisms and the National Science Foundation under grant CNS-0540033. The authors acknowledge the important support of DDDAS research by Dr. Frederica Darema of NSF. During the course of this work we benefited from advice and comments of many colleagues, we mention in particular, C. Bajaj, J. C. Browne, I. Babuška, J. Bass, L. Bidaut, L. Demkowicz, S. Goswami, A. Hawkins, S. Khoshnevis, B. Kwon, and S. Prudhomme. The authors would like to thank Drs. Ashok Gowda and Roger McNichols from BioTex Inc. for providing the Visualase®System and altering the software so that it may be remotely controlled. The authors would also like to thank the ITK [24], Paraview [23], PETSc [2], TAO [3], libMesh [26], and CUBIT [34] communities for providing truly enabling software for real-time scientific computation and visualization.

References

1. D. E. Atkins, K. K. Droegemeier, S. I. Feldman, H. Garcia-Molina, M. L. Klein, D. G. Messerschmitt, P. Messina, J. P. Ostriker, and M. H. Wright. Revolutionizing science and engineering through cyberinfrastructure: Report of the national science foundation blue-ribbon advisory panel on cyberinfrastructure. Technical report, National Science Foundation, 2003.

2. Satish Balay, William D. Gropp, Lois C. McInnes, and Barry F. Smith. Petsc users manual. Technical Report ANL-95/11 - Revision 2.1.5, Argonne National Laboratory, 2003.
3. Steven J. Benson, Lois Curfman McInnes, Jorge Moré, and Jason Sarich. TAO user manual (revision 1.8). Technical Report ANL/MCS-TM-242, Mathematics and Computer Science Division, Argonne National Laboratory, 2005. http://www.mcs.anl.gov/tao.
4. A Carpentier, D Chauvet, V Reina, K Beccaria, D Leclerq, R J McNichols, A Gowda, P Cornu, and J Y Delattre. MR-guided LITT for recurrent glioblastomas. *Lasers in Surgery and Medicine*, 2012.
5. A. Carpentier, RJ McNichols, RJ Stafford, J. Itzcovitz, JP Guichard, D. Reizine, S. Delaloge, E. Vicaut, D. Payen, A. Gowda, et al. Real-time magnetic resonance-guided laser thermal therapy for focal metastatic brain tumors. *Neurosurgery*, 63(1 Suppl 1):8, 2008.
6. Alexandre Carpentier, Roger J McNichols, R Jason Stafford, Jean-Pierre Guichard, Daniel Reizine, Suzette Delaloge, Eric Vicaut, Didier Payen, Ashok Gowda, and Bernard George. Laser thermal therapy: Real-time MRI-guided and computer-controlled procedures for metastatic brain tumors. *Lasers in Surgery and Medicine*, November 2011.
7. C.K. Charny. Mathematical models of bioheat transfer. *Adv. Heat Trans.*, 22:19–155, 1992.
8. D J Curry, A Gowda, R J McNichols, and A A Wilfong. MR-guided stereotactic laser ablation of epileptogenic foci in children. *Epilepsy & Behavior*, 2012.
9. K. R. Diller, J. T. Oden, C. Bajaj, J. C. Browne, J. Hazle, I. Babuška, J. Bass, L. Bidaut, L. Demkowicz, A. Elliott, Y. Feng, D. Fuentes, S. Goswami, A. Hawkins, S. Khoshnevis, B. Kwon, S. Prudhomme, and R. J. Stafford. *Advances in Numerical Heat Transfer*, volume 3: Numerical Implementation of Bioheat Models and Equations, chapter 9: Computational Infrastructure for the Real-Time Patient-Specific Treatment of Cancer. Taylor & Francis Group, 2008.
10. A.M. Elliott, J. Schwartz, J. Wang, A.M. Shetty, C. Bourgoyne, D.P. ONeal, J.D. Hazle, and R.J. Stafford. Quantitative comparison of delta P1 versus optical diffusion approximations for modeling near-infrared gold nanoshell heating. *Medical Physics*, 36:1351, 2009.
11. S. Fahrenholtz, R. J. Stafford, J. Hazle, and D. Fuentes. Generalised polynomial chaos-based uncertainty quantification for planning mrglitt procedures. *International Journal of Hyperthermia*, 29(4):324–335, 2013.
12. Y. Feng and D. Fuentes. Model-Based Planning and Real-Time Predictive Control for Laser-Induced Thermal Therapy. *Inter. Journal Hyperthermia*, 27(8):751–761, 2011. invited review.
13. Y. Feng, D. Fuentes, A. Hawkins, J. Bass, M. N. Rylander, A. Elliott, A. Shetty, R. J. Stafford, and J. T. Oden. Nanoshell-mediated laser surgery simulation for prostate cancer treatment. *Engineering with Computers*, 25(1):3–13, 2009.
14. Y. Feng, J. T. Oden, and M.N. Rylander. A statistical thermodynamics based cell damage models and its validation in vitro. *J. Biomech. Eng.*, 130(041016):1–10, 2008.
15. Y. Feng, M. N. Rylander, J. Bass, J. T. Oden, and K. Diller. Optimal design of laser surgery for cancer treatment through nanoparticle-mediated hyperthermia therapy. In *NSTI-Nanotech 2005*, volume 1, pages 39–42, 2005.
16. D. Fuentes. *Computational Modeling and Real-Time Control of Patient-Specific Laser Treatment of Prostate Cancer*. PhD thesis, The University of Texas at Austin, 2008.
17. D. Fuentes, R. Cardan, R. J. Stafford, J. Yung, G. D. Dodd III, and Y. Feng. High Fidelity Computer Models for Prospective Treatment Planning of RF Ablation with *in vitro* Experimental Correlation. *J. of Vascular and Interventional Radiology*, 21(11):1725–1732, 2010.
18. D. Fuentes, A. Elliott, J. S. Weinberg, A. Shetty, J. D. Hazle, and R. J. Stafford. An Inverse Problem Approach to Recovery of In-Vivo Nanoparticle Concentrations from Thermal Image Monitoring of MR-Guided Laser Induced Thermal Therapy. *Ann. BME.*, 41(1):100–111, 2013.
19. D. Fuentes, Y. Feng, A. Elliott, A. Shetty, R. J. McNichols, J. T. Oden, and R. J. Stafford. Adaptive Real-Time Bioheat Transfer Models for Computer Driven MR-guided Laser Induced Thermal Therapy. *IEEE Trans. Biomed. Eng.*, 57(5), 2010. Cover Page.
20. D. Fuentes, J. T. Oden, K. R. Diller, J. Hazle, A. Elliott, , A. Shetty, and R. J. Stafford. Computational modeling and real-time control of patient-specific laser treatment cancer. *Ann. BME.*, 37(4):763, 2009. DOI 10.1007/s10439-008-9631-8.

21. D. Fuentes, C. Walker, A. Elliott, A. Shetty, J. Hazle, and R. J. Stafford. MR Temperature Imaging Validation of a Bioheat Transfer Model for LITT. *International Journal of Hyperthermia*, 27(5):453–464, 2011. Cover Page.
22. D. Fuentes, J. Yung, J. D. Hazle, J. S. Weinberg, and R. J. Stafford. Kalman Filtered MR Temperature Imaging for Laser Induced Thermal Therapies. *Trans. Medical Imaging*, 31(4):984–994, 2012. Special Issue on Interventional Imaging.
23. A. Henderson and J. Ahrens. *The ParaView Guide*. Kitware, 2004.
24. L. Ibanez, W. Schroeder, L. Ng, and J. Cates. *The ITK Software Guide*. Kitware, Inc. ISBN 1-930934-15-7, http://www.itk.org/ItkSoftwareGuide.pdf, second edition, 2005.
25. P R Jethwa, J C Barrese, A Gowda, A Shetty, and S F Danish. Magnetic Resonance Thermometry-Guided Laser-Induced Thermal Therapy for Intracranial Neoplasms: Initial Experience. *Neurosurgery*, 71:ons133—-ons145, 2012.
26. B.S. Kirk and JW Peterson. libMesh-a C++ Finite Element Library. *CFDLab. URL http://libmesh. sourceforge. net*, 2003.
27. J. Liu, L. Zhu, and L. Xu. Studies on the three-dimensional temperature transients in the canine prostate during transurethral microwave thermal therapy. *J. Biomech. Engr*, 122:372–378, 2000.
28. J. T. Oden, K. R. Diller, C. Bajaj, J. C. Browne, J. Hazle, I. Babuška, J. Bass, L. Demkowicz, Y. Feng, D. Fuentes, S. Prudhomme, M. N. Rylander, R. J. Stafford, and Y. Zhang. Dynamic data-driven finite element models for laser treatment of prostate cancer. *Num. Meth. PDE,*, 23(4):904–922, 2007.
29. H. H. Pennes. Analysis of tissue and arterial blood temperatures in the resting forearm. *J. Appl. Physiol.*, 1:93–122, 1948.
30. SA Prahl, M. Keijzer, SL Jacques, and AJ Welch. A Monte Carlo model of light propagation in tissue. *Dosimetry of Laser Radiation in Medicine and Biology*, 155:102–111.
31. M.N. Rylander. *Design of Hyperthermia Protocols for Inducing Cardiac Protection and Tumor Destruction by Controlling Heat Shock Protein Expression*. PhD thesis, The University of Texas at Austin, 2005.
32. R. J. Stafford, R. E. Price, C. J. Diederich, M. Kangasniemi, L. E. Olsson, and J. D. Hazle. Interleaved echo-planar imaging for fast multiplanar magnetic resonance temperature imaging of ultrasound thermal ablation therapy. *Journal of Magnetic Resonance Imaging*, 20(4):706–714, 2004.
33. R Jason Stafford, Anil Shetty, Andrew M Elliott, Sherry a Klumpp, Roger J McNichols, Ashok Gowda, John D Hazle, and John F Ward. Magnetic resonance guided, focal laser induced interstitial thermal therapy in a canine prostate model. *The Journal of urology*, 184(4):1514–20, October 2010.
34. T. Blacker *et al.* Cubit Users Manual, 2008. `http://cubit.sandia.gov/documentation`.
35. A. Wambersie and T. Landberg. ICRU Report 62: Prescribing, Recording and Reporting Photon Beam Therapy (Supplement to ICRU Report 50). *Bethesda, MD: International Commission on Radiation Units and Measurements*, 1999.
36. A. J. Welch and M. J. C. van Gemert. *Optical-Thermal Response of Laser-Irradiated Tissue*. New York: Plenum Press, 1995.
37. E. H. Wissler. Pennes' 1948 paper revisited. *J. Appl. Physiol.*, 85:35–41, 1998.